



This is a repository copy of *Fully-integrated transformer with asymmetric leakage inductances for a bidirectional resonant converter*.

White Rose Research Online URL for this paper:  
<https://eprints.whiterose.ac.uk/188638/>

Version: Accepted Version

---

**Proceedings Paper:**

Ansari, S.A., Davidson, J.N. [orcid.org/0000-0002-6576-3995](https://orcid.org/0000-0002-6576-3995) and Foster, M.P. (2022) Fully-integrated transformer with asymmetric leakage inductances for a bidirectional resonant converter. In: 11th International Conference on Power Electronics, Machines and Drives (PEMD 2022). PEMD 2022 - The 11th International Conference on Power Electronics, Machines and Drives, 21-23 Jun 2022, Newcastle, UK (hybrid conference). IET Digital Library , pp. 260-265. ISBN 9781839537189

<https://doi.org/10.1049/icp.2022.1014>

---

© 2022 IET. This is an author-produced version of a paper accepted for publication in PEMD 2022. Uploaded in accordance with the publisher's self-archiving policy.

**Reuse**

Items deposited in White Rose Research Online are protected by copyright, with all rights reserved unless indicated otherwise. They may be downloaded and/or printed for private study, or other acts as permitted by national copyright laws. The publisher or other rights holders may allow further reproduction and re-use of the full text version. This is indicated by the licence information on the White Rose Research Online record for the item.

**Takedown**

If you consider content in White Rose Research Online to be in breach of UK law, please notify us by emailing [eprints@whiterose.ac.uk](mailto:eprints@whiterose.ac.uk) including the URL of the record and the reason for the withdrawal request.



[eprints@whiterose.ac.uk](mailto:eprints@whiterose.ac.uk)  
<https://eprints.whiterose.ac.uk/>

# Fully-integrated Transformer with Asymmetric Leakage Inductances for a Bidirectional Resonant Converter

Sajad A Ansari<sup>1\*</sup>, Jonathan N Davidson<sup>2</sup>, Martin P Foster<sup>3</sup>

<sup>1,2,3</sup>Department of Electronic and Electrical Engineering, The University of Sheffield, Sheffield, UK  
\*sarabansari1@sheffield.ac.uk

**Keywords:** BIDIRECTIONAL CONVERTER, CLLLC RESONANT CONVERTER, INTEGRATED TRANSFORMER, MAGNETIC SHUNT.

## Abstract

In this paper, a new design for an integrated planar transformer is presented which can provide asymmetric leakage inductance in primary and secondary sides. Therefore, the proposed integrated transformer can be used in bidirectional resonant converters in which the primary and secondary inductors have different values. To achieve a precise, high leakage inductance for the primary and secondary sides, two magnetic shunts are inserted into a planar transformer. In the proposed topology, flexible magnetic sheets which can be cut easily are used as the magnetic shunts, leading the design process to high flexibility. The analysis, design and modelling of the proposed integrated transformer are presented in detail. It is shown that the magnetising inductance can be determined by regulating the length of an inserted air gap inserted between two E-cores. In addition, the leakage inductance of the primary and secondary sides can be regulated separately by the length of air gaps inserted within the magnetic shunts. The theoretical analysis is verified by finite element analysis and the operation of the proposed integrated transformer is demonstrated while it is used in a CLLLC bidirectional converter.

## 1 Introduction

Nowadays, the development of energy storage systems (ESSs) especially household storage systems has gained popularity since they can restrain power fluctuation of the grid [1, 2]. In energy storage systems, the power needs to be transferred from the grid to batteries and vice versa [3-5]. Therefore, a bidirectional AC-DC converter followed by a bidirectional DC-DC converter are required in these systems. The DC-DC converters play an important role in these systems since they manage the power flow between DC bus and batteries and also boost or decrease the voltage level. Hence, it is preferred that the DC-DC converters have high efficiency and power density and low cost [6-8].

The bidirectional pulse-width-modulated (PWM) DC-DC converters suffer from low efficiency due to high switching losses and cannot be operated at high-frequency, leading to low power density [9, 10]. On the other hand, the resonant converters benefit from soft-switching capability inherently and therefore they can be a good candidate for bidirectional power transfer in energy storage systems [11]. Amongst resonant converters, the LLC converter is one of the most popular because of its advantages such as soft-switching capability, integration of magnetic components and high efficiency at wide input and output voltage range. However,

this topology is only suitable for unidirectional power transfer since its operation principle changes noticeably in bidirectional power transfer mode and its soft-switching capability cannot be attained for both directions [12].

A lot of research has been done to adopt the LLC resonant converter for bidirectional power transfer. A bidirectional LLC converter which has unity turns ratio and symmetric components in primary and secondary sides of its transformer is proposed in [13]. The topology presented in [13] still benefits from all advantages of the LLC resonant converter while it can transfer power in any direction. However, the gain of the converter must be unity in this topology. Therefore, this topology is not suitable for battery charging applications in which the battery voltage varies significantly during the whole charging process. Another design methodology for LLC-type converter is proposed in [14], to overcome the issue of wide input and output voltage ranges.

The converter proposed in [14] is a bidirectional CLLLC resonant converter which is based on an LLC-type converter with an extra inductor and capacitor in the secondary side. It can operate with wide input and output voltage ranges and soft-switching capability. Therefore, the design methodology presented in [14] can be a suitable choice for battery charging applications and is considered in this paper.

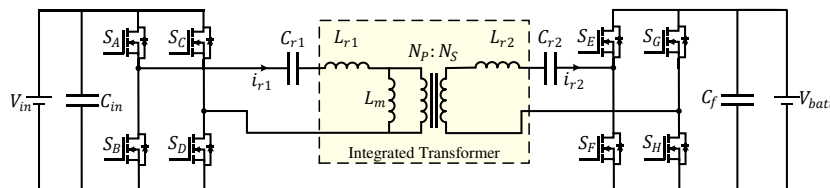


Fig. 1 Schematic of a bidirectional CLLLC resonant converter.

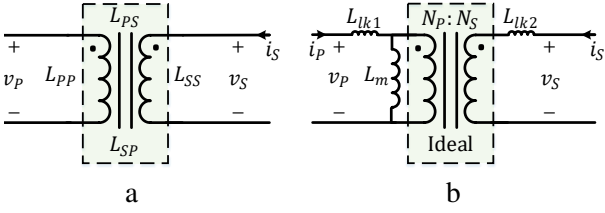


Fig. 2 The equivalent circuit of (a) coupled inductor, (b) transformer.

The topology of a CLLC resonant converter is shown in Fig. 1. It can be seen that this converter needs four magnetic components, which makes the converter giant and costly. However, these magnetic components can be integrated into a single transformer to enhance the converter power density and efficiency and decrease its cost.

Many methods have been introduced for the integration of magnetic components in an LLC resonant converter [15]. Amongst these methods, inserted-shunt integrated planar transformer has gained popularity since this method benefits from many advantages such as precise estimation of leakage inductance, achieving high leakage inductance and simple manufacturing [16-22]. In this method, the leakage inductance can be increased in both primary and secondary sides by inserting different types of magnetic shunts. However, the inserted-shunt integrated transformer can be only applied in a CLLC converter when its magnetic components are symmetric in both primary and secondary sides. Therefore, the presented introduced inserted-shunt integrated transformers are not suitable for the converter proposed in [14] and other similar converters in which primary and secondary magnetic components are not symmetric.

In this paper, in order to address the aforementioned issues with inserted-shunt integrated planar transformers, a new topology is proposed which can provide asymmetric leakage inductance in the primary and secondary sides of an integrated transformer. In the proposed topology, two magnetic shunts are inserted between two E-cores and the primary and secondary windings are separated by being located above and below the magnetic shunts, respectively. In addition, flexible magnetic sheets which can be cut easily are used as the magnetic shunts in the proposed topology, leading the design process to high flexibility. The design and modelling of the proposed topology will be provided. It is shown that the magnetising inductance, and primary and secondary leakage inductances are decoupled from each other in the design process and can be regulated separately. Finite element analysis (FEA) results are presented to confirm the modelling and design guideline of the proposed topology. Finally, the operation of the proposed transformer while it is used in a bidirectional CLLC resonant converter is investigated.

The paper is organized as follows: The basic definition of magnetising and leakage inductances and modelling of the proposed integrated transformer is presented in section 2. In section 3, the simulation results are provided to confirm modelling and the operation of the proposed transformer is investigated when it is used in a CLLC

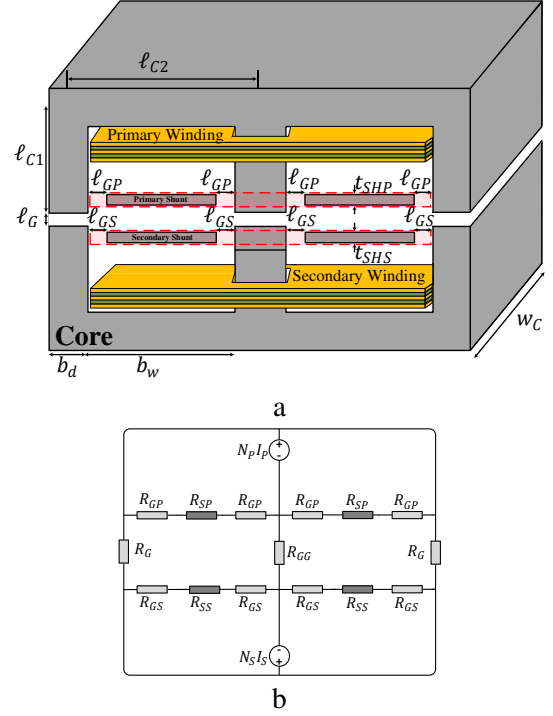


Fig. 3 The proposed integrated transformer. (a) Schematic. (b) Reluctance model.

resonant converter. Finally, a conclusion for this work is provided in section 4.

## 2. Proposed integrated transformer with asymmetric leakage inductances

### 2.1 Basic definition of magnetising and primary and secondary leakage inductances

The equivalent circuit of a coupled inductor is presented in Fig. 2(a) and relationship between its voltages and currents may be presented as (1) [23, 24].

$$\begin{bmatrix} v_p \\ v_s \end{bmatrix} = \begin{bmatrix} L_{PP} & L_{PS} \\ L_{SP} & L_{SS} \end{bmatrix} \frac{d}{dt} \begin{bmatrix} i_p \\ i_s \end{bmatrix} \quad (1)$$

where  $L_{PS}$  and  $L_{SP}$  are mutual inductances and  $L_{PP}$  and  $L_{SS}$  are primary and secondary self-inductances, respectively. Another equivalent circuit for a coupled inductor can be also defined which is presented in Fig. 2(b) and relationship between its voltages and currents may be expressed as (2).

$$\begin{bmatrix} v_p \\ v_s \end{bmatrix} = \begin{bmatrix} L_{lk1} + L_m & \frac{N_s}{N_p} L_m \\ \frac{N_s}{N_p} L_m & L_{lk2} + \frac{N_s^2}{N_p^2} L_m \end{bmatrix} \frac{d}{dt} \begin{bmatrix} i_p \\ i_s \end{bmatrix} \quad (2)$$

where  $N_p$  and  $N_s$  are turns number of primary and secondary windings and  $L_m$  is magnetising inductance which may be expressed as (3).

$$L_m = \frac{N_p}{N_s} L_{PS} \quad (3)$$

The mutual inductance may be obtained by (4).

$$L_{PS} = \frac{N_s}{N_p} \phi_{PS} \quad (4)$$

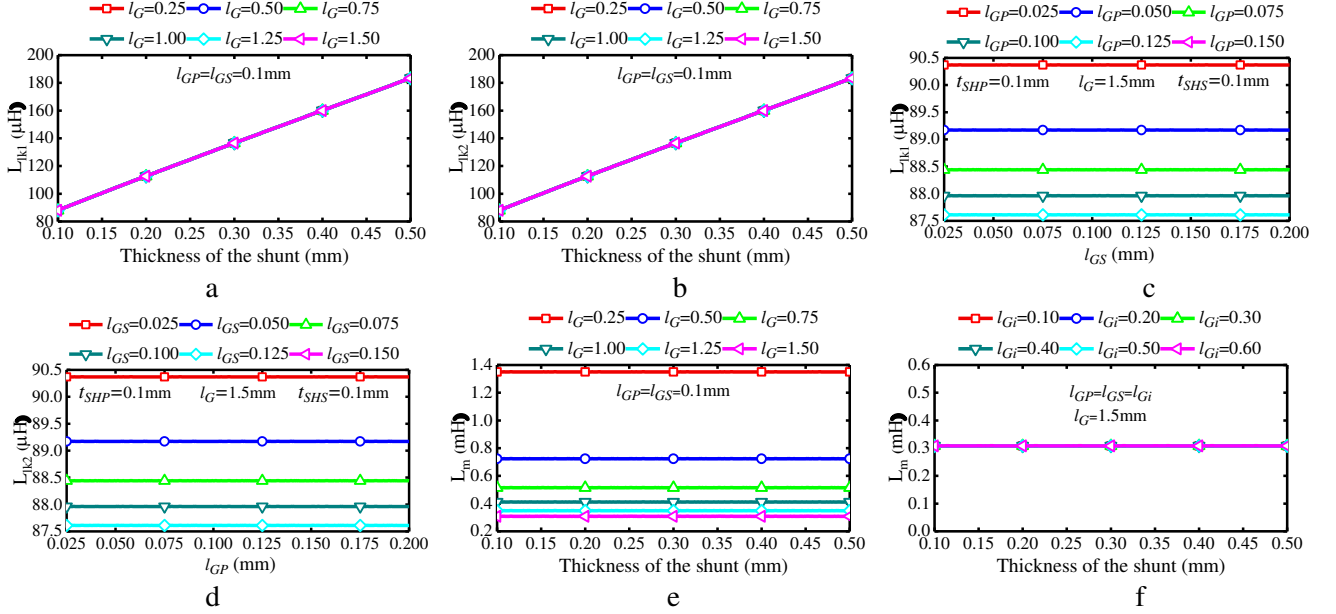


Fig. 4 The calculated leakage and magnetising inductances for different thickness of the shunts and air-gap lengths. (a)  $L_{lik1}$  versus  $t_{SHP,S}$  and  $l_G$ . (b)  $L_{lik2}$  versus  $t_{SHP,S}$  and  $l_G$ . (c)  $L_{lik1}$  versus  $l_{GS}$  and  $l_{GP}$ . (d)  $L_{lik2}$  versus  $l_{GP}$  and  $l_{GS}$ . (e)  $L_m$  versus  $l_G$  and  $t_{SHP,S}$ . (f)  $L_m$  versus  $l_{GS,P}$  and  $t_{SHP,S}$ . Core: E58/11/38-3F4,  $N_p=40$ ,  $N_s=40$ .

where  $\phi_{PS}$  is the mutual flux generated by the primary winding. From (3) and (4), the magnetizing inductance can be achieved as (5).

$$L_m = \frac{N_p}{I_p} \phi_{PS} \quad (5)$$

Therefore, the mutual flux needs to be calculated for calculation of the magnetising inductance. The primary self-inductance may be expressed as (6).

$$L_{pp} = \frac{N_p^2}{\mathcal{R}} \quad (6)$$

where  $\mathcal{R}$  is the core reluctance. The primary and secondary leakage inductances can be achieved by (7) and (8), respectively [23, 24].

$$L_{lik1} = L_{pp} - L_m \quad (7)$$

$$L_{lik2} = L_{ss} - \frac{N_s^2}{N_p^2} L_m \quad (8)$$

## 2.2 Magnetising and leakage inductances calculation

The schematic of the proposed shunt-inserted integrated transformer with asymmetric leakage inductances is shown in Fig. 3 (a). As shown, two magnetic shunts are inserted between two E-cores and primary and secondary windings are separated by being located at the above and below of magnetic shunts. Two air gaps are inserted in between each E-core and its related shunt to regulate the leakage inductances. In addition, an air gap is inserted between the E-cores to regulate the magnetising inductance. The equivalent reluctance model of the proposed topology is presented in Fig. 3(b). In this model, the permeability of the core is assumed to be much larger than the permeability of the air and therefore the reluctance of the air gap and shunts only need to be considered. In addition, it is assumed that leakage flux is very small in the window area and can be ignored. In Fig. 3(b),  $\mathcal{R}_{SP}$  and  $\mathcal{R}_{SS}$  are

reluctances of the shunts and  $\mathcal{R}_{GP}$ ,  $\mathcal{R}_{GS}$ ,  $\mathcal{R}_G$  and  $\mathcal{R}_{GG}$  are the reluctances of the air gaps and may be expressed as follows:-

$$\mathcal{R}_{SP} = \frac{b_w - 2l_{GP}}{\mu_0 \mu_s t_{SHP} w_c} \quad (9)$$

$$\mathcal{R}_{SS} = \frac{b_w - 2l_{GS}}{\mu_0 \mu_s t_{SHS} w_c} \quad (10)$$

$$\mathcal{R}_{GP} = \frac{l_{GP}}{\mu_0 t_{SHP} w_c} \quad (11)$$

$$\mathcal{R}_{GS} = \frac{l_{GS}}{\mu_0 t_{SHS} w_c} \quad (12)$$

$$\mathcal{R}_G = \frac{l_G}{\mu_0 b_d w_c} \quad (13)$$

$$\mathcal{R}_{GG} = \frac{l_G}{\mu_0 A_c} \quad (14)$$

where  $\mu_0$  is the permeability of the air and  $\mu_s$  is the relative permeability of the shunt,  $A_c$  is the core effective cross-sectional area and the definition of other quantities can be found in Fig. 3(a).

According to Fig. 3(b), the mutual fluxes  $\phi_{PS}$  and  $\phi_{SP}$  may be expressed as (15) and (16), respectively.

$$\phi_{PS} = \frac{N_p I_p}{\frac{\mathcal{R}_G}{2} + \mathcal{R}_{GG}} \quad (15)$$

$$\phi_{SP} = \frac{N_s I_s}{\frac{\mathcal{R}_G}{2} + \mathcal{R}_{GG}} \quad (16)$$

Applying (15) in (5), the magnetising inductance may be calculated as

$$L_m = \frac{N_p^2}{\frac{\mathcal{R}_G}{2} + \mathcal{R}_{GG}} \quad (17)$$

In addition, the self-inductance of the primary and secondary windings may be obtained as (18) and (19), respectively.

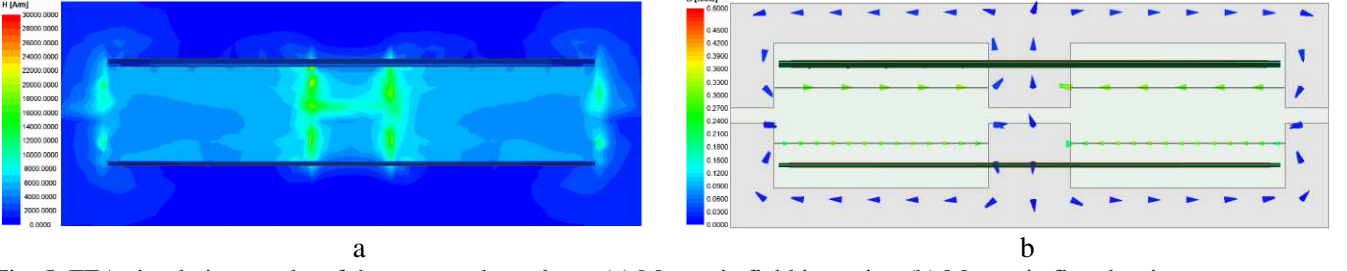


Fig. 5 FEA simulation results of the proposed topology. (a) Magnetic field intensity. (b) Magnetic flux density vectors.

$$L_{PP} = \frac{N_p^2 \left( \frac{\mathcal{R}_{SP}}{2} + \mathcal{R}_{GP} + \mathcal{R}_G + 2\mathcal{R}_{GG} \right)}{\left( \frac{\mathcal{R}_{SP}}{2} + \mathcal{R}_{GP} \right) \left( \frac{\mathcal{R}_G}{2} + \mathcal{R}_{GG} \right)} \quad (18)$$

$$L_{SS} = \frac{N_s^2 \left( \frac{\mathcal{R}_{SS}}{2} + \mathcal{R}_{GS} + \mathcal{R}_G + 2\mathcal{R}_{GG} \right)}{\left( \frac{\mathcal{R}_{SS}}{2} + \mathcal{R}_{GS} \right) \left( \frac{\mathcal{R}_G}{2} + \mathcal{R}_{GG} \right)} \quad (19)$$

From (7), (8), (17), (18) and (19), the primary and secondary leakage inductances may be calculated as (20) and (21), respectively.

$$L_{lk1} = \frac{2N_p^2}{\frac{\mathcal{R}_{SP}}{2} + \mathcal{R}_{GP}} \quad (20)$$

$$L_{lk2} = \frac{2N_s^2}{\frac{\mathcal{R}_{SS}}{2} + \mathcal{R}_{GS}} \quad (21)$$

The calculated magnetising inductance and primary and secondary leakage inductances versus thickness of the shunt for different air gaps are shown in Figs. 4(a)-(f), respectively. It is clear that the magnetising inductance is mainly affected by the air gap which is inserted in between E-cores ( $\ell_G$ ) and does not change noticeably for different thicknesses of the shunts. On the other hand, the leakage inductances are mainly affected by the thickness of the shunts and the air gap between them and E-cores ( $\ell_{GP}$  and  $\ell_{GS}$ ). As presented in Fig. 4 and from (20) and (21), the primary leakage inductance is only affected by the primary shunt and the secondary leakage inductance is only affected by the secondary shunt. Therefore, the magnetising inductance and primary and secondary leakage inductances are decoupled from each other in the design process and can be determined separately.

Commercially available flexible magnetic sheets like Flexfield IFL/IBF, which is available from the thickness of 0.05mm, can be used as the magnetic shunts and the thickness

of the shunts can be also increased by inserting them in parallel, which increases the flexibility of the design.

### 3. Simulation Results

In this section, FEA results of a designed integrated transformer with specifications presented in Table 1 are provided to confirm the theoretical analysis. The transformer is designed to be used in an exemplar bidirectional CLLC resonant converter with characteristic presented later in Table 2.

The magnetic field intensity of the proposed transformer is shown in Fig. 5(a). As shown, the magnetic field intensity in the shunts air gaps ( $\ell_{GP}$  and  $\ell_{GS}$ ) is higher than the window area which proves the fact that leakage inductance is mainly affected by the magnetic shunt and leakage flux going through the window area is negligible. In addition, the air gap inserted in between E-cores ( $\ell_G$ ) has the highest magnetic field intensity and therefore the magnetising inductance is highly affected by the length of this air gap. The magnetic flux density vectors of the proposed topology are shown in Fig. 5(b). The main flux goes through the vertical legs and some of the flux goes through the magnetic shunts in order to realise the leakage inductance.

The leakage and magnetising inductances of the proposed topologies measured by FEA and calculated from equations (17), (20) and (21) are shown in Figs. 6(a) and (b), respectively. As shown, there is only a small discrepancy between calculated and measured values which confirms the accuracy of theoretical analysis. The introduced assumptions for modelling of the proposed transformer such as negligible fringing effect, negligible reluctance of the cores and

Table 1 Proposed structure's specification

Symbol	Parameter	Value
$N_p$	Primary turns number	40
$N_s$	Secondary turns number	10
$S$	Shunt material	IFL04
$\ell_G$	Transformer air gap	1.50 mm
$\ell_{GP}$	Distance between shunt and cores	0.10 mm
$\ell_{GS}$	Distance between shunt and cores	0.10 mm
$C$	Core material of E58/11/38	3F4
$t_{SHP}$	Thickness of primary shunt	0.05 mm
$t_{SHS}$	Thickness of secondary shunt	0.10 mm

Table 2 The designed CLLC Converter's Specification

Symbol	Parameter	value
$N_p: N_s$	Turns ratio	40:10
$L_m$	Magnetising inductance	310 $\mu$ H
$L_{r1}$	Primary resonant inductance	082 $\mu$ H
$L_{r2}$	Secondary resonant inductance	5.75 $\mu$ H
$C_{r1}$	Primary resonant capacitance	031 nF
$C_{r2}$	Secondary resonant capacitance	500 nF
$V_{in}$	Input voltage	350-450 V
$V_{out}$	Output voltage	080-120 V
$P_{out}$	Output power	1 kW
$f_s$	Switching frequency	70-135 kHz

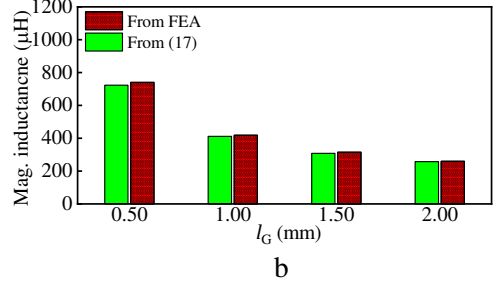
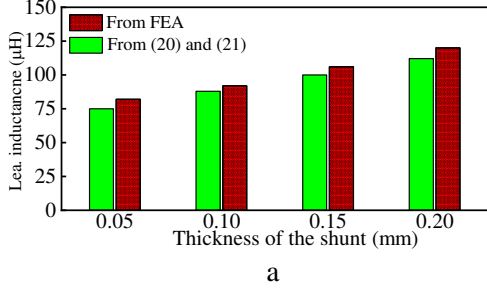


Fig. 6 Modelling validation by FEA. (a) Leakage inductance ( $\ell_G = 1.5mm$ ). (b) Magnetising inductance ( $t_{SHP} = t_{SHS} = 0.05mm$ ).  $N_p=40$ ,  $N_s=40$ ,  $\ell_{GP} = \ell_{GS} = 0.1mm$ .

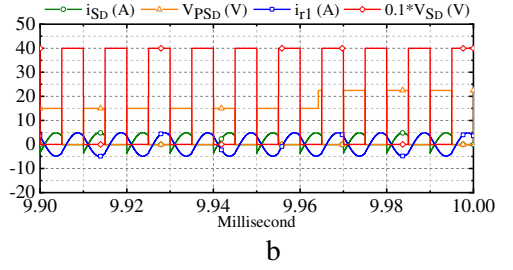
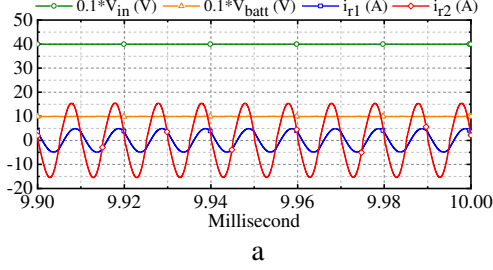


Fig. 7 Simulation results for BCM. (a) Input voltage,  $V_{in}$ , battery voltage,  $V_{batt}$ , primary current,  $i_{r1}$ , and secondary current,  $i_{r2}$ . (b) D switch voltage,  $V_{SD}$ , D switch pulse voltage,  $V_{PSD}$ , primary current,  $i_{r1}$ , and D switch current,  $i_{SD}$ .

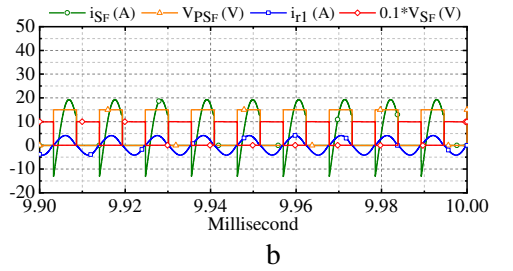
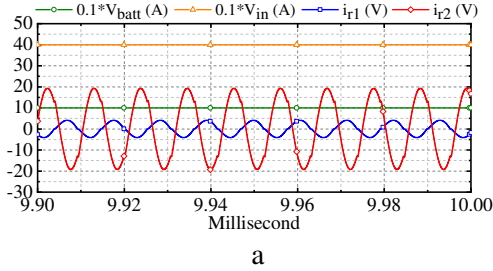


Fig. 8 Simulation results for RM. (a) Input voltage,  $V_{in}$ , battery voltage,  $V_{batt}$ , primary current,  $i_{r1}$ , and secondary current,  $i_{r2}$ . (b) F switch voltage,  $V_{SF}$ , F switch pulse voltage,  $V_{PSF}$ , primary current,  $i_{r1}$ , and F switch current,  $i_{SF}$ .

negligible flux of window area explain the reason of the small discrepancy between calculated and measured values.

The operation of the proposed integrated transformer needs to be investigated when it is used in a bidirectional CLLC resonant converter. Therefore, the simulation results of a bidirectional CLLC resonant converter while its magnetic components are integrated in the proposed transformer for battery charging mode (BCM) and regeneration mode (RM) are presented in Figs. 7 and 8, respectively. As shown, the converter operates properly in both modes and the switches are turned on at zero-voltage (ZVS) since the drain-to-source voltage of switches drops to zero and then its gate voltage increases. It has to be mentioned that the bidirectional CLLC converter is designed according to the design procedure outlined in [14] and its specifications are presented in Table 2.

## 4 Conclusion

In this paper, a new topology for shunt-inserted integrated transformers is proposed which can provide asymmetric leakage inductances for primary and secondary sides. The proposed topology is simple and only two magnetic shunts are

inserted in between two planar E-cores. In addition, since the commercially available flexible magnetic sheets can be used as the magnetic shunts, the proposed topology can be implemented with high flexibility in the design process. The design guideline and modelling of the proposed topology is provided and is confirmed by FEA. In addition, an exemplar bidirectional CLLC resonant converter is designed and the operation of the proposed transformer is investigated when it is used in the designed bidirectional converter. It is shown that the proposed transformer can integrate all the four magnetic components of an asymmetric bidirectional CLLC resonant converter into a single planar transformer.

## 5 References

- [1] Y. Zuo, X. Pan, and C. Wang, "A Reconfigurable Bidirectional isolated LLC Resonant Converter for Ultra-Wide Voltage-gain Range applications," *IEEE Transactions on Industrial Electronics*, 2021.
- [2] A. Mizani, S. A. Ansari, A. Shoulaie, J. N. Davidson, and M. P. Foster, "Single-active switch high-voltage gain DC-DC converter using a non-coupled inductor," *IET Power Electronics*, vol. 14, no. 3, pp. 492-502, 2021.

- [3] Y. Zhang, D. Zhang, J. Li, and H. Zhu, "Bidirectional LCLL Resonant Converter With Wide Output Voltage Range," *IEEE Transactions on Power Electronics*, vol. 35, no. 11, pp. 11813-11826, 2020.
- [4] A. Mirzaee, S. Arab Ansari, and J. Shokrollahi Moghani, "Single switch quadratic boost converter with continuous input current for high voltage applications," *International Journal of Circuit Theory and Applications*, vol. 48, no. 4, pp. 587-602, 2020.
- [5] S. A. Ansari, J. N. Davidson, and M. P. Foster, "COMPARATIVE EVALUATION OF Si MOSFET-BASED SOFT-SWITCHED DC-DC CONVERTERS AND GaN HEMT-BASED HARD-SWITCHED DC-DC CONVERTERS," 2021.
- [6] A. Soni and A. K. Dhakar, "Bi-Directional CLLC Resonant Converter with Integrated Planar Transformer for Energy Storage Systems," in *IECON 2020 The 46th Annual Conference of the IEEE Industrial Electronics Society*, 2020: IEEE, pp. 4255-4260.
- [7] S. A. Ansari and J. S. Moghani, "Soft switching flyback inverter for photovoltaic AC module applications," *IET Renewable Power Generation*, vol. 13, no. 13, pp. 2347-2355, 2019.
- [8] S. Arab Ansari, J. S. Moghani, and M. Mohammadi, "Analysis and implementation of a new zero current switching flyback inverter," *International Journal of Circuit Theory and Applications*, vol. 47, no. 1, pp. 103-132, 2019.
- [9] S. A. Ansari, J. N. Davidson, and M. P. Foster, "Evaluation of silicon MOSFETs and GaN HEMTs in soft-switched and hard-switched DC-DC boost converters for domestic PV applications," *IET Power Electronics*, vol. 14, no. 5, pp. 1032-1043, 2021.
- [10] S. A. Ansari and J. S. Moghani, "A novel high voltage gain noncoupled inductor SEPIC converter," *IEEE Transactions on Industrial Electronics*, vol. 66, no. 9, pp. 7099-7108, 2018.
- [11] Y. Liao *et al.*, "Single-stage DAB-LLC hybrid bidirectional converter with tight voltage regulation under DCX operation," *IEEE Transactions on Industrial Electronics*, vol. 68, no. 1, pp. 293-303, 2020.
- [12] W. Chen, P. Rong, and Z. Lu, "Snubberless bidirectional DC-DC converter with new CLLC resonant tank featuring minimized switching loss," *IEEE Transactions on industrial electronics*, vol. 57, no. 9, pp. 3075-3086, 2009.
- [13] J.-H. Jung, H.-S. Kim, M.-H. Ryu, and J.-W. Baek, "Design methodology of bidirectional CLLC resonant converter for high-frequency isolation of DC distribution systems," *IEEE Transactions on Power Electronics*, vol. 28, no. 4, pp. 1741-1755, 2012.
- [14] Z. U. Zahid, Z. M. Dalala, R. Chen, B. Chen, and J.-S. Lai, "Design of bidirectional DC-DC resonant converter for vehicle-to-grid (V2G) applications," *IEEE Transactions on Transportation Electrification*, vol. 1, no. 3, pp. 232-244, 2015.
- [15] S. Stegen and J. Lu, "Structure comparison of high-frequency planar power integrated magnetic circuits," *IEEE transactions on magnetics*, vol. 47, no. 10, pp. 4425-4428, 2011.
- [16] M. Li, Z. Ouyang, B. Zhao, and M. A. Andersen, "Analysis and modeling of integrated magnetics for LLC resonant converters," in *IECON 2017-43rd Annual Conference of the IEEE Industrial Electronics Society*, 2017: IEEE, pp. 834-839.
- [17] M. Li, Z. Ouyang, and M. A. Andersen, "High-frequency LLC resonant converter with magnetic shunt integrated planar transformer," *IEEE Transactions on Power Electronics*, vol. 34, no. 3, pp. 2405-2415, 2018.
- [18] S. Arab Ansari, J. Davidson, and M. Foster, "Fully-integrated Planar Transformer with a Segmental Shunt for LLC Resonant Converters," *IEEE Transactions on Industrial Electronics*, 2021, doi: 10.1109/TIE.2021.3116574.
- [19] S. A. Ansari, J. N. Davidson, and M. P. Foster, "Fully-Integrated Solid Shunt Planar Transformer for LLC Resonant Converters," *IEEE Open Journal of Power Electronics*, vol. 3, pp. 26 - 35, 2021, doi: 10.1109/OJPEL.2021.3137016.
- [20] S. A. Ansari, J. N. Davidson, M. P. Foster, and D. A. Stone, "Design and analysis of a Fully-integrated planar transformer for LCLC resonant converters," in *2021 23rd European Conference on Power Electronics and Applications (EPE'21 ECCE Europe)*, 2021: IEEE, pp. P. 1-P. 8.
- [21] S. A. Ansari, J. N. Davidson, and M. P. Foster, "Analysis, Design and Modelling of Two Fully-Integrated Transformers with Segmental Magnetic Shunt for LLC Resonant Converters," in *IECON 2020 The 46th Annual Conference of the IEEE Industrial Electronics Society*, 2020: IEEE, pp. 1273-1278.
- [22] S. A. Ansari, J. Davidson, and M. Foster, "Inserted-shunt Integrated Planar Transformer with Low Secondary Leakage Inductance for LLC Resonant Converters," *IEEE Transactions on Industrial Electronics*, 2022.
- [23] A. Taylor, J. Lu, L. Zhu, K. H. Bai, M. McAmmond, and A. Brown, "Comparison of SiC MOSFET-based and GaN HEMT-based high-efficiency high-power-density 7.2 kW EV battery chargers," *IET Power Electronics*, vol. 11, no. 11, pp. 1849-1857, 2018.
- [24] S. De Simone, C. Adragna, and C. Spini, "Design guideline for magnetic integration in LLC resonant converters," in *2008 International Symposium on Power Electronics, Electrical Drives, Automation and Motion*, 2008: IEEE, pp. 950-957.